Desalination and Water Treatment
www.deswater.com

doi: 10.5004/dwt.2018.21920

109 (2018) 90–103
March

Application of artificial neural network and random forest methods for modeling simultaneous adsorption of safranin-O and methyl violet dyes onto modified pine cone powder

Motahare Ashrafi, Ghadamali Bagherian*, Mansour Arab Chamjangali, Nasser Goudarzi

Faculty of Chemistry, Shahrood University of Technology, Shahrood, P.O. Box 36155-316, Iran, Tel. +98 23 32395441; emails: Gh_Bagherian@shahroodut.ac.ir (G. Bagherian), mot.ashrafi@gmail.com (M. Ashrafi), arabe51@yahoo.com (M. Arab Chamjangali), goudarzi10@yahoo.com (N. Goudarzi)

Received 25 August 2017; Accepted 17 January 2018

ABSTRACT

In the present work, a new carboxylate-functionalized pine cone was prepared using isopropylidene malonate in a solvent-free reaction. It was then characterized by the FT-IR, X-ray diffraction, scanning electron microscopy, and Brunauer–Emmett–Teller analysis techniques. The performance of the modified adsorbent was investigated for the removal of the safranin-O (SO) and methyl violet (MV) dyes from the single and binary solutions. The maximum adsorption capacity for SO and MV in the single solution was 208.0 and 225.0 mg/g, respectively, whereas these values were, respectively, 112.30 and 116.7 mg/g for the binary solution. This value is much higher than those reported by some other researchers. The kinetic studies revealed that this bio-sorption is a chemisorption process. In continuation, the experimental factors involving the initial solution pH, adsorbent dosage, dye concentration, and contact time were used as the input variables to the artificial neural network (ANN) and random forest (RF) models to predict the removal percentage of SO and MV in the binary mixture. The validation of these models was tested using a test set of 81 data points. The statistical parameters involved in the prediction of the removal percentage of the test set confirmed that the ANN model had a substantially better and a more accurate prediction with respect to the RF model.

Keywords: Random forest; Artificial neural network; Methyl violet; Safranin-O

1. Introduction

Nowadays more than one hundred thousand types of commercial dyes are produced and utilized in the world [1]. It has been reported that a large amount of them are lost during their production and dyeing procedure, which create a significant volume of dye-containing effluents [2]. Of these, safranin-O (SO) and methyl violet (MV) are two kinds of cationic dyes that are extensively utilized as the coloring agents in the textile, paper, leather, and pharmaceutical industries [3]. In spite of their widespread applications, the major disadvantages associated with these colored effluents are skin sensitivity, eye infections, and stomach pain [3]. Dyes are the first and most undesirable pollutants of water [4,5]. Therefore, their removal from effluents prior to their discharge to the natural environment is of great importance. So far different methods have been offered to treat wastewaters contaminated by these colored compounds. Owing to its simplicity of design and suitability for diverse types of dyes, adsorption using eco-friendly materials has been recognized as a promising technique [5,6,7]. Activated carbon, as the most commonly used adsorbent, has two major drawbacks. Its first shortcoming is that it is prepared from expensive materials such as wood. Its second drawback is that its regeneration is difficult [7,8]. Recently, much attention has been given to bio-adsorbents due to their low cost, easy availability, and low toxicity. Nevertheless, the adsorption capacities of most reported bio-adsorbents are low. Chemical modification

* Corresponding author.

can introduce some functional groups such as the carboxyl and amine ones onto the surface of bio-sorbents to improve their adsorption capacity [9,10]. In the present work, isopropylidene malonate was used as modifier because of the following reasons: (i) it is non-toxic, stable, commercially available; (ii) it can easily react with nucleophilic functional groups such as hydroxyl and amine; (iii) its melting point is low and can participate in a solvent-free reaction, (iv) the yield of its reaction is often above 80% [11,12].

It should be noted that the prediction of water quality, as the output of a water treatment plant, is difficult because the input water quality changes continuously [13]. In a water treatment plant, the output of an adsorption process, which is the removal percentage or adsorbed amount of pollutant per unit mass of the adsorbent, is severely dependent on the experimental parameters such as the initial pH, dye concentration, contact time, and adsorbent dose [5,13]. Unfortunately, the accomplishment of an experimental testing is often costly and time consuming. Modeling using computational techniques can solve this problem. Modeling is a simplification of reality and is very suitable to obtain information about how a process behaves without carrying out practical experiments [14–16]. Nowadays different computational methods such as the artificial neural network (ANN), neuro-fuzzy inference system, and random forest (RF) methods are employed to model the adsorption processes [5,15,16]. These methods are very suitable when the complexity of the underlying mechanism of the process is very high and cannot be explained by statistical techniques [17]. In this work, the simultaneous adsorption of SO and MV onto modified pine cone was modeled using the ANN and RF techniques. The main advantage of these methods is that mathematical explanation is not required for the phenomena involved in the process, and the relationship between the input and output data is obtained using the examples given to it [5,13]. Also using this method, one can obtain information about the relative importance of the parameters driving the sorption process [5,17].

In order to investigate the adsorption behavior of a dye mixture, it is necessary to determine the concentrations of the dyes present in the dye mixture simultaneously [2]. Among the most widely used analytical methods, the spectrophotometric techniques are cheaper and simpler. However, overlapping absorption peaks limit the use of the traditional spectrophotometric techniques [2,18]. Fortunately, the multivariate calibration methods expand the applicability of spectrophotometric methods for a multi-component analysis [19]. The advantage of a multi-component analysis using multivariate calibration is its speed in the determination of the components present in a mixture, avoiding the preliminary separation step [20]. Among the different methods available for a multivariate calibration, partial least squares regression (PLSR) can be used to analyze the data with strongly co-linear (correlated), noisy and numerous *X*-variables [21]. Because in this technique, the new predictor variables, termed as the latent variables, are created as the linear combination of the original predictor variables, and consequently, the dimensionality of data is reduced. This method requires a calibration set, where the relationship between the spectra (X) and the component concentration (Y) is realized from a set of reference samples, followed by a prediction step in which the results obtained from the calibration are used to determine the component concentrations using the sample UV-visible spectrum [19,22].

Therefore the main objectives of the current work were as follow: (i) determination of the concentration of the cationic SO and MV dyes in a binary mixture using the PLS method; (ii) modification of pine cone powder (PCP) with carboxylic groups, and characterization of the modified PCP by FT-IR spectroscopy, X-ray diffraction (XRD), and scanning electron microscopy (SEM); (iii) assessment of the applicability of the modified pine cone for the removal of the dyes; (iv) analysis of the isotherms and kinetics participating in the sorption procedure; (v) evaluation of the recovery of the proposed adsorbent; (vi) modeling the sorption behavior of the cited dyes at different experimental conditions using the ANN and RF methods.

2. Experimental

2.1. Materials, instruments, and software

Pine cone (PC) was collected from the campus of Shahrood University of Technology, Shahrood, Iran. SO (molecular formula = $C_{20}H_{19}N_4Cl$, molecular weight = 350.85, maximum wavelength = 518 nm) and MV (molecular formula = $C_{24}H_{28}N_3Cl$, molecular weight = 393.96, maximum wavelength = 586 nm), 2,2-isopropylidene malonate, hydrochloric acid (HCl), sodium hydroxide (NaOH), sodium chloride (NaCl), sodium bicarbonate ($NaHCO_3$), and ethanol (C_2H_6O) were supplied from Merck (Germany). 1 g/L of the stock solution of each dye (SO and MV) was prepared, and the required diluted solutions were prepared daily by diluting the appropriate volumes of their stock solutions with double-distilled water. The pH measurements were made using a Metrohm 744 pH meter. To record the UV-visible spectra, a double beam UV-visible spectrophotometer (Rayleigh UV-2601) was used. The surface features and functional groups of the carboxyl-modified pine cone powder (CMPCP) were investigated using a scanning electron microscope (MIRAW TESCAN) and an FT-IR spectrophotometer (WQF-520), respectively. The XRD patterns were recorded using Unisantis XRD diffractometer (XMD300, Germany). A gas sorption system (Belsorp-Max, BEL Japan, Inc.) was used to determine the surface area and porosity of the adsorbent before and after modification. The PLS, ANN, and RF programs were written in the MATLAB (Mathworks Inc., Natick, MA, USA) software and run on a personal computer.

2.2. Preparation of adsorbent

PC is known to have a lot of hydroxyl groups that can react with 2,2-isopropylidene malonate to create ester bonds, introducing carboxyl groups to PC [12]. In this regard, PC was ground in a domestic grinder and treated with sodium hydroxide to remove impurities such as wax, lignin, and natural fats [6]. Then 5 g of the alkaline-treated bio-sorbent that was neutralized was mixed with 15 g of isopropylidene malonate and heated at 110°C in a round-bottom flask equipped with a reflux condenser in an oil bath, stirred magnetically. After 4 h, the mixture was cooled at room temperature and rinsed with distilled water and sodium hydrogen bicarbonate solution to wash and neutralize the modified

biomass. Finally, the CMPCP was oven dried at 110°C for the subsequent experiments. The chemical reaction involved is demonstrated in Fig. 1.

2.3. Simultaneous analysis of SO and MV in their binary mixture

For the simultaneous analysis of SO and MV, a binary mixture of these two dyes (4 mg/L) was prepared and its zero-order absorption spectrum was recorded (Fig. 2). As one can see in this figure, due to the spectral overlapping, an accurate determination of the SO and MV dyes in their binary mixture was not possible by the direct UV-visible absorbance measurement. To overcome this problem, the PLS multivariate calibration method was used. A calibration set of binary mixtures was designed using a square experimental domain with seven levels for the two dyes. The concentration of each dye in the standard solutions lay in their linear dynamic range. This subset was used to optimize the number of latent variables. The second subset (an external test set with seven samples) was employed for validation of the constructed model. A combination of the calibration set and the test set is demonstrated in Tables 1 and 2, respectively.

The optimum number of latent variables (scores or factors) for each dye was determined using the leave-one-out cross-validation technique [19,23]. Minimization of root mean square error (RMSE) was selected as a criterion in the optimization process. This statistical parameter is defined as follows:

$$\mathrm{RMSE} = \sqrt{\frac{\sum\left(\hat{C}_i - C_i\right)^2}{n}} \tag{1}$$

where C_i is the theoretical concentration of analyte i, $\hat{C}_i$ is the estimated (predicted) concentration of analyte i, and n is the number of calibration samples. In this regard, RMSE was calculated for the first latent variable, which built the PLS model in the calibration step. Then the second latent variable was added and RMSE was computed again. For 1–25 latent variables (half the number of standards plus one [19]), the computations were reiterated. The number of latent variables giving the minimum RMSE was chosen for modeling. This process was applied for each dye in the prediction solutions, and the optimum number of latent variables was estimated. In our particular case, the number of latent variables of 2 was obtained as the optimum value for each dye (Fig. 3). In continuation, the accuracy of the PLS method was checked using the external test, which was not present in the calibration set, and the results obtained are tabulated in Table 2. The results

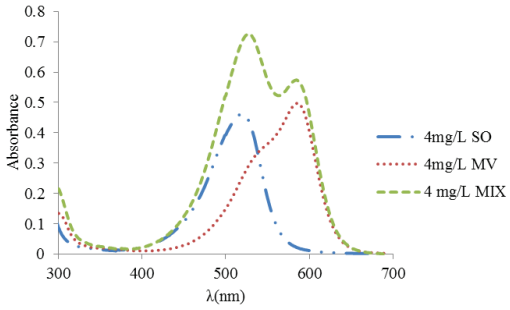

Fig. 2. Zero-order absorption spectra for SO and MV in single and binary solutions.

Table 1
Combination of different mixtures of SO and MV used in calibration set

Sample	SO (mg/L)	MV (mg/L)	Sample	SO (mg/L)	MV (mg/L)
1	0.20	0.20	26	0.20	10.00
2	10.00	2.00	27	2.00	4.00
3	0.20	4.00	28	6.00	2.00
4	8.00	0.20	29	0.20	0.50
5	0.20	8.00	30	0.50	10.00
6	6.00	10.0	31	2.00	2.00
7	0.20	2.00	32	4.00	2.00
8	0.50	0.50	33	8.00	10.00
9	10.00	6.00	34	0.20	6.00
10	0.50	2.00	35	2.00	0.20
11	0.50	4.00	36	0.50	0.20
12	10.00	10.00	37	10.00	0.20
13	8.00	4.00	38	6.00	6.00
14	6.00	0.50	39	0.50	6.00
15	4.00	10.00	40	10.00	8.00
16	4.00	8.00	41	2.00	10.00
17	2.00	0.50	42	4.00	0.20
18	8.00	2.00	43	0.50	8.00
19	2.00	6.00	44	8.00	0.50
20	2.00	8.00	45	10.00	0.50
21	6.00	0.20	46	8.00	8.00
22	6.00	8.00	47	10.00	4.00
23	4.00	6.00	48	8.00	6.00
24	4.00	0.50	49	4.00	4.00
25	6.00	4.00			

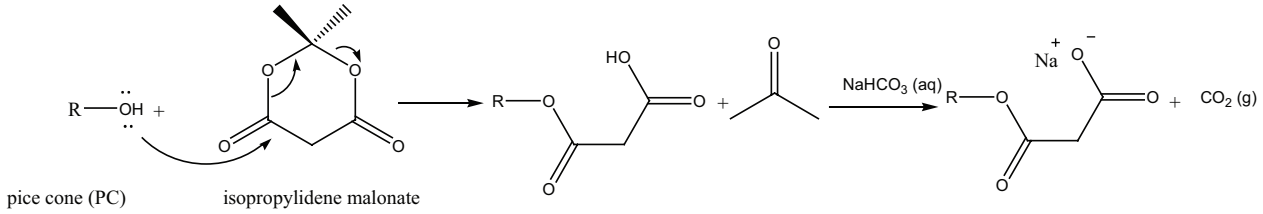

Fig. 1. Reaction route used to obtain CMPCP.

obtained show that the PLS method can satisfactorily predict the concentration of dyes in their binary mixture solution. Therefore, for the subsequent experiments, the PLS method was used to determine the SO and MV concentrations in their binary mixture.

2.4. Batch dye adsorption studies

Dye adsorption studies were performed by mixing a known amount of the adsorbent with 50 mL of the dye solution of definite concentration in a series of 100-mL beakers in a single solution or a binary mixture of the dyes. The pH values for these solutions were adjusted, and then the solutions were agitated using a magnetic stirrer at 200 rpm at 25°C ± 2°C to investigate the effects of the parameters that influenced the adsorption process. Then at a pre-selected time interval, a certain amount of the sample (2 mL) was centrifuged at 3,500 rpm for 1 min. The dye concentration in the supernatant solution was analyzed spectrophotometrically. The SO and MV concentrations in the single and binary solutions were determined using the direct calibration and PLSR methods, respectively. The individual removal percentage (R, %) and the adsorbed amount of each dye per weight of the adsorbent at equilibrium ($q_{e,i}$) can be calculated using Eqs. (2) and (3), respectively [14].

$$R = \frac{(C_{0,i} - C_{e,i})}{C_{0,i}} \times 100 \quad (2)$$

Table 2
Values for real and predicted concentrations of SO and MV in their binary mixture obtained by PLS method

Theoretical (mg/L)		Measured (mg/L)		Error	
C_{SO}	C_{MV}	C_{SO}	C_{MV}	SO	MV
0.20	1.00	0.20	1.07	0.00	0.07
0.30	0.30	0.33	0.32	0.03	0.02
3.00	3.00	2.91	2.85	–0.09	–0.15
5.00	3.00	5.14	3.02	0.14	0.02
7.00	7.00	6.53	6.99	–0.47	–0.01
7.00	5.00	7.19	5.33	0.19	0.33
6.00	5.00	6.23	4.65	0.23	–0.45

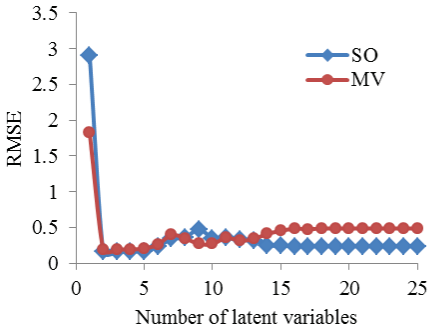

Fig. 3. RMSE of training data vs. number of latent variables.

$$q_{e,i} = \frac{(C_{0,i} - C_{e,i})V}{W} \quad (3)$$

where $C_{0,i}$ is the initial dye concentration (mg/L), $C_{e,i}$ is the residual dye concentration at equilibrium (mg/L), V is the volume of the solution (L), and W is the mass of the dry adsorbent

3. Results and discussion

3.1. Characterization of PC and CMPCP

In order to identify the functional groups on CMPCP and the mechanism of adsorption between the adsorbent and adsorbate [24], the FT-IR spectra for PC and CMPCP (Fig. 4) were recorded in the range of 400–4,000 cm^{-1}. Before adsorption, the broad band at around 3,418 cm^{-1} can be attributed to the O–H stretching vibration of the hydroxyl groups in cellulose. The well-defined peaks at 2,931 cm^{-1} and 1,460 cm^{-1} are characteristics of the C–H bond stretching and bending vibrations of the methyl and methylene groups, respectively [25,26]. The peaks observed at 1,730 and 1,624 cm^{-1} are related to the stretching vibration of the C=O bond due to the non-ionic and ionic carboxyl groups, respectively [25]. As it can be seen in Figs. 4(C) and (D), for CMPCP in the acidic or basic form, two new peaks appeared at 1,159 and 1,748 cm^{-1}. The former can be assigned to the C–O stretching vibration in the ester [27–29] and the latter can be attributed to the C=O bond, which is the overlap of the absorption at 1,750 cm^{-1} of C=O bond in the ester and that at 1,712 cm^{-1} of carboxylic acid [27,28]. After treatment of the adsorbent with $NaHCO_3$, the asymmetric and symmetric stretching vibrations of carboxylate groups (COO^-) at 1,608 and 1,380 cm^{-1} increased. This indicates that some of the carboxylic groups were converted to the carboxylate ions. Also the absence of peaks at 1,792 and 1,753 cm^{-1} for CMPCP confirmed that the modified adsorbent is free from the unreacted isopropylidene malonate.

The crystallography of PCP and CMPCP was determined using X-ray diffractograms (Fig. 5). For PCP, the main characteristic peaks for cellulose (I) were detected at $2\theta = 15.7°$, 21.3°, and 34.4° [30]. This spectrum confirms that PCP basically has the structure of crystalline cellulose. After modification, a small shift in the cellulosic peaks and a significant decrease in their intensities were observed, which could be attributed to the reduction in the crystalline cellulose content [30,31].

Fig. 6 shows the SEM micrographs for PCP and CMPC. The surface texture of powdered pine cone prior

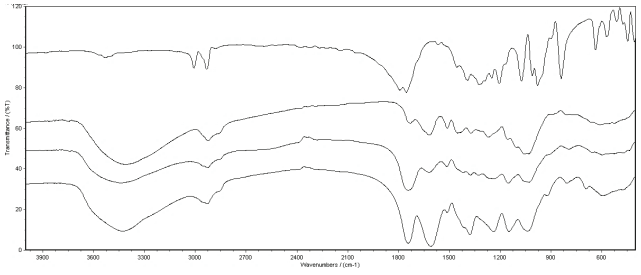

Fig. 4. FT-IR spectra for (A) 2,2-isopropylidene malonate, (B) PC, (C) CMPCP in acidic form, and (D) CMPCP in basic form.

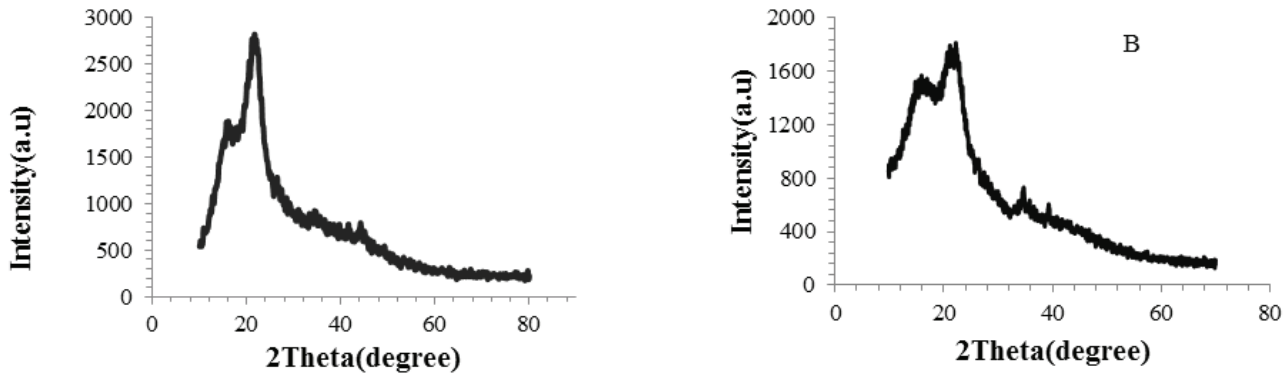

Fig. 5. X-ray diffractograms for (A) PC and (B) CMPCP.

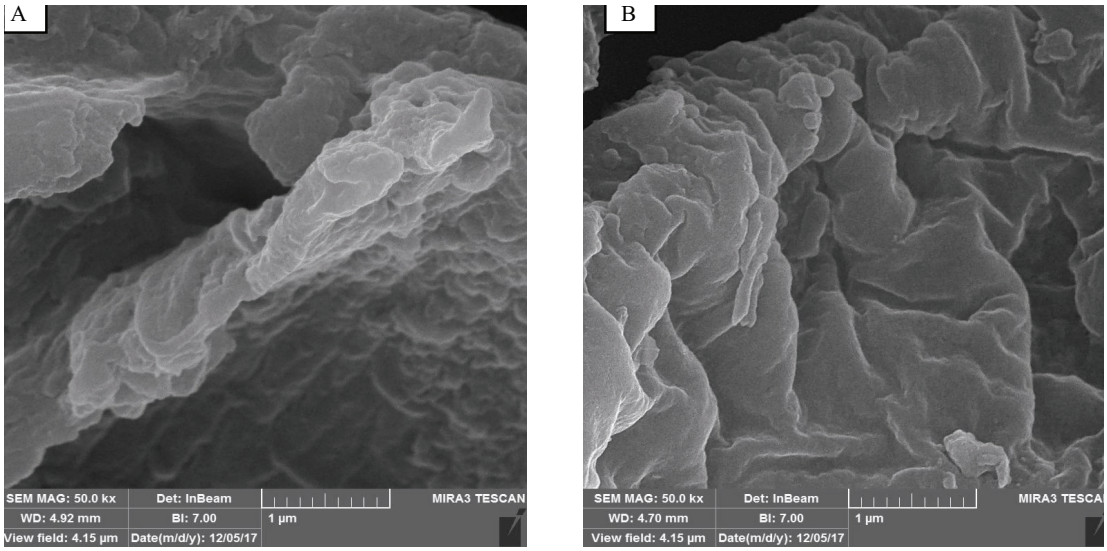

Fig. 6. SEM images for (A) PCP and (B) CMPCP.

to modification was observed to be smooth and less undulated, while the surface morphology of powder pine cone after modification was observed to be more undulated. The Brunauer–Emmett–Teller (BET) analysis data were given in Table 3. The specific surface area for CMPCP (0.323 m^2/g), which was calculated using the BET equation, was 2.4 times as much as that of PCP (0.132 m^2/g), and could provide a larger contact area to adsorb more dye molecules. Moreover, the average pore diameter of CMPCP was 55.5 nm, indicating that CMPCP was a mesoporous material [14].

Table 3
Physico-chemical parameters for PC and CMPC

Parameter	Adsorbent	
	PC	CMPC
BET surface area (m^2/g)	0.132	0.323
Total pore volume (cm^3/g)	0.00051	0.0044
Mean pore diameter (nm)	15.51	55.52
Micropore volume (cm^3/g)	0.030	0.073

3.2. Effect of initial pH on adsorption of SO and MV dyes

Since the solution pH can affect the surface charges of the adsorbent as well as the degree of ionization of the adsorbate, it is considered as a key parameter in an adsorption procedure [25,32]. In this work, the effect of the initial pH value on the adsorption of the SO and MV dyes onto CMPCP was investigated by mixing 50 mL of 50 mg/L of each dye solution with 0.015 g of CMPCP at various pH values in the range of 3–9, and their removal percentage was given in Fig. 7. According to the results obtained, adsorption of the dyes onto CMPCP is controlled by a pH-dependent mechanism. This behavior suggests that the grafted carboxyl groups (–COOH) are probably responsible for the adsorption of the cationic dyes. The pK_a values accounted for the fact that the carboxyl groups are between 3.5 and 5.5 [25,27]. Consequently, due to the protonation of these functional groups at an acidic pH, the sorption of cationic species decreases. However, at higher pH values, they are in the deprotonated form (COO^-), and interact effectively with the cationic dye molecules, and subsequently, the removal

percentage increases. As it could be seen in Fig. 7, a little amount of adsorption was observed in a highly acidic medium. This observation suggests that the other interactions such as the Van der Waals forces, hydrogen bonding between the deprotonated amine groups ($-N(CH_3)_2$) in the dye molecules, and the hydroxyl group of COOH present in the adsorbent surface are responsible for the adsorption of the dye molecules in highly acidic media.

3.3. Effect of contact time

The removal of SO and MV vs. contact time was surveyed to specify the adsorption equilibrium time. Plot of the experimental data (Fig. 8) indicate that the adsorption process involves two steps. The first step displays a fast adsorption, whereas the second one shows a gradual pattern until the equilibrium is established. The high amount of adsorbed dye molecules in the primary stage was due to the number of available active sites present in the surface layer of the bio-adsorbent [14,33]. After this stage, the active sites are gradually occupied by the dye molecules and do not lead to significant differences in the adsorption rate. This short time required to achieve the equilibrium implies that the proposed adsorbent has a potential for its application in the removal of textile dyes.

The adsorption kinetics of the dyes in the single and binary systems was analyzed by the pseudo-first order and pseudo-second order rate models (as the most well-known ones). The pseudo-first order equation based on the equilibtium data is generally expressed as [34]:

$$\log(q_e - q_t) = \log q_e - \frac{k_1 t}{2.303} \tag{4}$$

in which the variables q_e and q_t are the adsorbed amounts of a dye at equilibrium (mg/g) and time t (min), respectively, and k_1 (min^{-1}) is the adsorption rate constant. The values for k_1 and q_e were computed using the slope and intercept of the straight-line plots of $\log(q_e - q_t)$ against t, respectively. As demonstrated in Table 4, the calculated q_e ($q_{e,cal}$) values for both dyes in the single and binary systems were far away from the experimental ones. This result confirms that the adsorption reaction is not related to pseudo-first order kinetic model. Thus it was essential to apply another model to fit the experimental data. Therefore, the adsorption data were related to the pseudo-second order kinetic model, expressed as follows [34,35]:

$$\frac{t}{q_t} = \frac{1}{k_2 q_e^2} + \frac{1}{q_{eq}} t \tag{5}$$

The experimental data showed a better agreement with the pseudo-second order kinetic model for both dyes in terms of $R^2 > 0.99$. Furthermore, the $q_{e,cal}$ values from the pseudo-second order model were more consistent with the $q_{e,exp}$ values (Table 4). For this reason, it can be concluded that the pseudo-second order kinetic model is more appropriate to describe the adsorption behavior of the cited dyes. The compatibility with the pseudo-second order kinetic model shows that adsorption of the dye molecules onto the adsorbent is chemisorption [5], and confirms that the functional groups are involved in the adsorption process.

The pseudo-first order and pseudo-second order models could not forecast the rate limiting step for the SO and MV

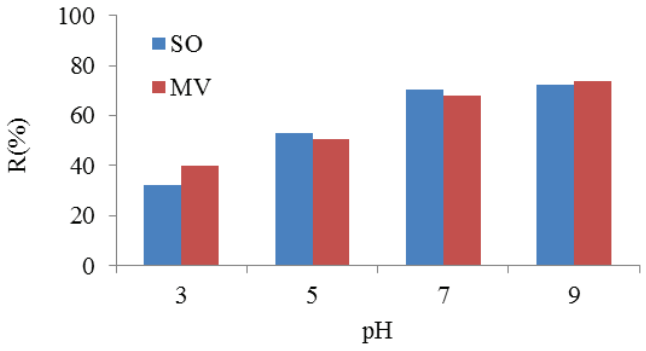

Fig. 7. Effect of pH on removal percentage of dye with 0.015 g CMPCP (50 mL of 50 mg/L of dye at 25°C ± 2°C and a contact time of 25 min).

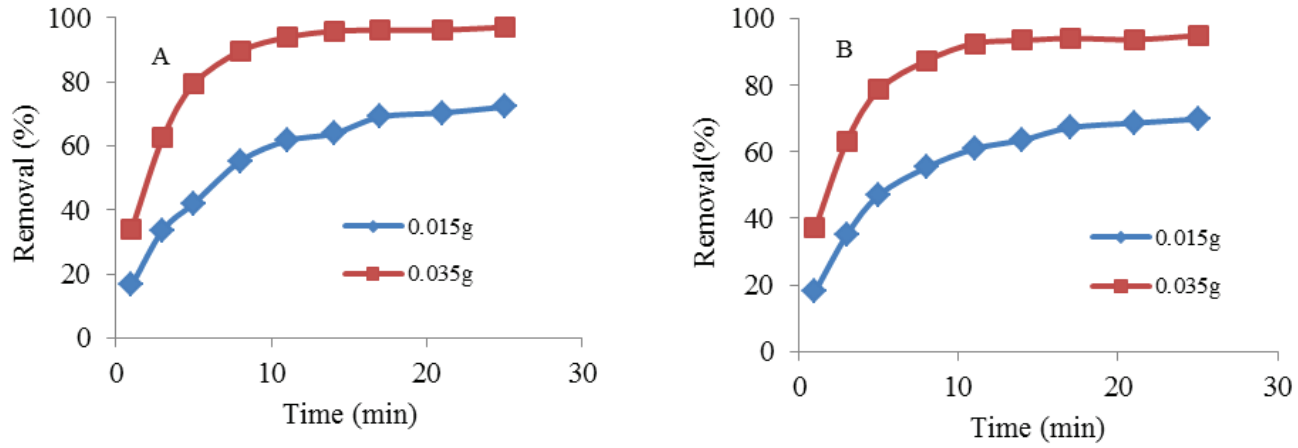

Fig. 8. Effect of contact time on removal percentage of dyes for different amounts of CMPCP (50 mL of 50 mg/L of (A) SO and (B) MV at pH = 7).

Table 4
Kinetic parameters involved in adsorption of SO and MV onto prepared adsorbent in single and binary systems[a]

System	C (mg/L)	Pseudo-first order				Pseudo-second order		
		$q_{e,exp}$ (mg/g)	$q_{e,cal}$ (mg/g)	k_1 (min^{-1})	R^2	$q_{e,cal}$ (mg/g)	k_2 (min/mg/g)	R^2
Single								
SO	50	69.62	29.18	0.187	0.9035	71.43	0.0187	0.9999
MV	50	67.09	23.53	0.232	0.8787	68.96	0.026	0.9997
Binary								
SO	50	66.1	44.86	0.241	0.9469	71.42	0.0083	0.9985
MV	50	63.47	39.25	0.23	0.9183	68.03	0.0099	0.9989

[a]Conditions: adsorbent dosage of 0.7 g/L and pH 7.0.

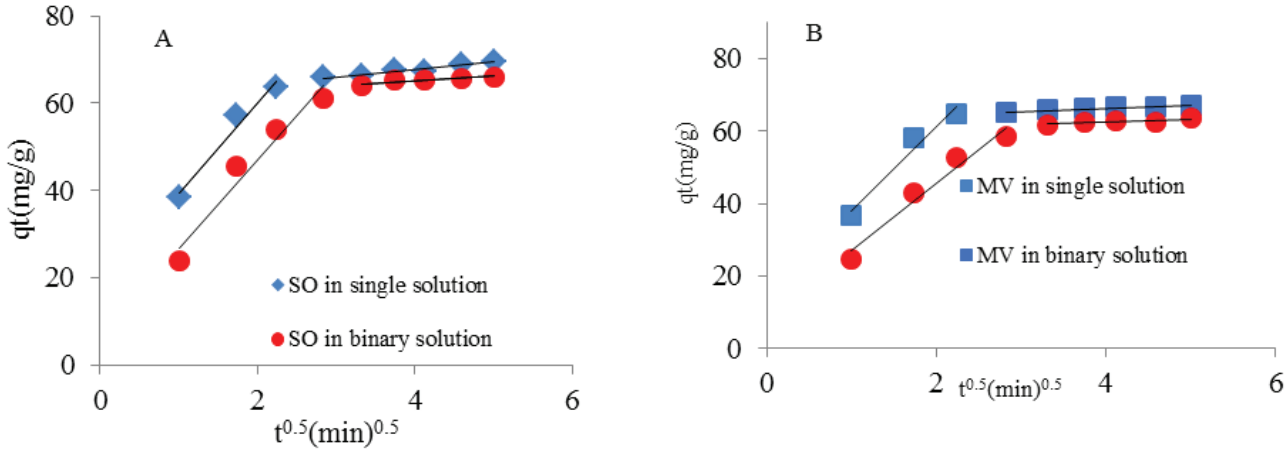

Fig. 9. Intra-particle diffusion plot for adsorption of SO and MV dyes onto 0.035 g of CMPCP (50 mL of 50 mg/L of dye concentration at pH = 7) in single and binary systems.

adsorption [36]. For this reason, the experimental data were analyzed by the intra-particle diffusion model, as follows:

$$q_t = k_d t^{\frac{1}{2}} + c \tag{6}$$

where k_d and c are the intra-particle diffusion rate constant and thickness of boundary layer, respectively. These values were acquired using the slope and intercept of the plot of q_t vs. $t^{1/2}$. Usually the intra-particle diffusion model contains two parts that are accredited to the phenomena such as the initial surface adsorption and the subsequent intra-particle diffusion [38]. If the value for c is zero (the respective plot of q_t against $t^{1/2}$ passes through the origin), and then the adsorption rate is controlled by the intra-particle diffusion. If the plots do not pass through the origin, this is indicative of some degrees of boundary layer control and shows that the intra-particle diffusion is not the only rate limiting step [37]. Based on the results obtained (Fig. 9; Table 5), in the adsorption of SO and MV onto the proposed bio-sorbent some other mechanism along with intra-particle diffusion is also involved.

3.4. Adsorption isotherms

Every adsorbent has a distinctive adsorption pattern for a specific adsorbate that can be stated using the mathematical equations called the sorption isotherms [38]. The applicability of a sorption process as a unit operation is determined using the physio-chemical parameters derived from these isotherms [39]. There are different isotherms available to describe the equilibrium data for the adsorption of dye onto a solid surface. In this work, the two most commonly used isotherm models, namely Langmuir and Freundlich, were chosen to evaluate the sorption of dyes onto CMPCP. The Langmuir model, which is the most frequently applied one, is based on the monolayer sorption, and can be explained as follows [37]:

$$q_{eq} = \frac{q_{max} k_l c_e}{1 + k_l c_e} \tag{7}$$

where q_{max}, k_l, and C_e are the maximum adsorption capacity (mg/g), Langmuir constant (L/mg), and concentration of adsorbate at equilibrium (mg/L), respectively.

The empirical Fruendlich isotherm was the second model employed in this work. This model, which is in the following form, describes a multi-layer adsorption on the adsorbent with a heterogeneous energy distribution of active sites [40].

$$q_{eq} = k_f c_e^{\frac{1}{n}} \tag{8}$$

Table 5
Parameters of intra-particle model in adsorption of SO and MV onto prepared adsorbent in single and binary systems

System[a]	C (mg/L)	Step 1			Step 2		
		$K_{id\ (step\ 1)}$(mg/g min½)	$c_{(step\ 1)}$ (mg/g)	$R^2_{(step\ 1)}$	$K_{id\ (step\ 2)}$ (mg/g min½)	$c_{(step\ 2)}$ (mg/g)	$R^2_{(step\ 2)}$
Single							
SO	50	20.71	18.80	0.9733	1.74	60.78	0.9429
MV	50	23.11	14.913	0.9639	0.8482	62.95	0.9569
Binary							
SO	50	20.26	6.64	0.9532	1.074	60.70	0.8087
MV	50	18.63	8.36	0.9530	0.78	59.35	0.8123

[a]Conditions: adsorbent dosage of 0.7 g/L and pH 7.0.

Table 6
Constants of isotherms computed by non-linear least squares method for adsorption of SO and MV in a single solution

Isotherms	Parameters	DYE	
		SO	MV
Freundlich	k_f	65.87	68.25
	n	3.56	3.41
	R^2	0.9430	0.9010
	RMSE	12.65	18.84
Langmuir	q_{max}	208.0	225.0
	k_l	0.245	0.2528
	R^2	0.9827	0.9739
	RMSE	6.035	9.70

In this equation, the variables q_{eq}, K_f, C_{eq}, and n are the equilibrium dye uptake (mg/g), relative sorption capacity ((mg/g) (L/mmol)$^{1/nF}$), equilibrium concentration of dye (mg/L), and sorption intensity, respectively.

The isotherm constants of each model were calculated using the non-linear least squares method in the Matlab software (Table 6). In this procedure, the statistical parameter RMSE, defined by Eq. (9), was applied as the criterion for evalution of the accuracy of the prediction and the quality of fittness of the experimental data. The model that had the lowest RMSE was chosen as a superior one.

$$\mathrm{RMSE} = \sqrt{\frac{\sum (q_{e,\exp} - q_{e,\mathrm{cal}})^2}{n}} \tag{9}$$

As one can understand from the results obtained (Fig. 10; Table 6), the Langmuir isotherm is more appropriate.

The extended-Langmuir adsorption isotherm and the Sheindorf–Rebuhn–Sheintuch isotherm (Freundlich-type multi-component isotherm) [14] were utilized to fit the equilibrium data of the SO and MV binary mixture.

$$q_{\mathrm{eq},j} = \frac{q_{\max,j} k_{l,j} c_{e,j}}{1 + \sum_{j=1}^{2} k_{l,j} c_{e,j}} \tag{10}$$

$$q^j_{e,,i} = k_{f,i} c_{e,i} (c_{e,i} + a c_{e,j})^{\left(\frac{1}{n_i} - 1\right)} \tag{11}$$

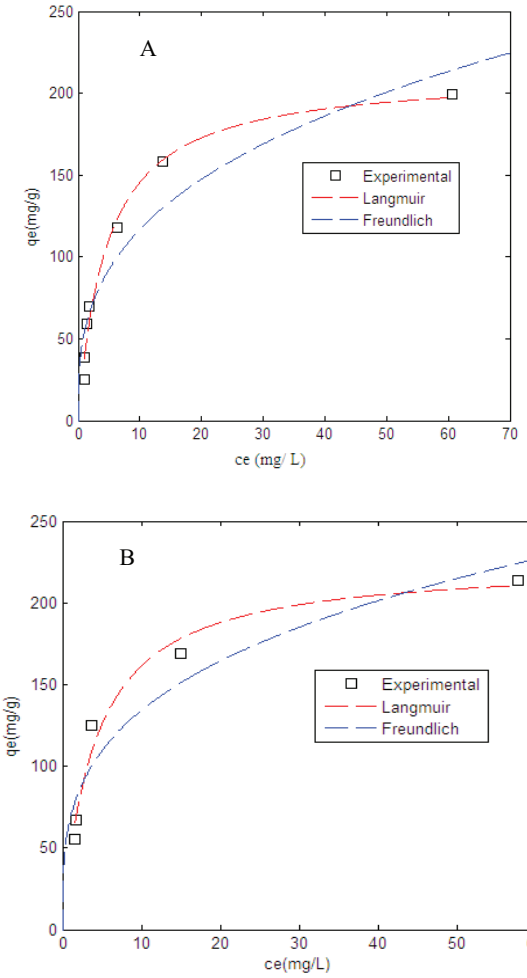

Fig. 10. Adsorption isotherm models for removal of (A) SO and (B) MV from single solutions.

where $q^j_{e,t}$, c_e, $q_{\max,j}$, and $k_{i,j}$ are the adsorbed amount of component i in the presence of component j, equilibrium concentration, maximum adsorption capacity (mg/g), and Langmuir constant (L/mg) for component j, respectively, acquired through a non-linear analysis employing the MATLAB software (Table 7). $k_{f,i}$ and n_i are the Freundlich isotherm constants derived from the single-component isotherm and θ_{ij} is the

competitive coefficient, which is estimated by a non-linear fitting. The results obtained (Table 7) show that the extended-Langmuir isotherm can describe the equilibrium data reasonably for both dyes in binary mixtures.

3.5. Effect of ionic strength

Due to the consumption of salt in the dyeing process, the effluents delivered from textile industries often contain a high amount of different ions. These ionic species can affect the bio-sorption ability of CMPCP. For this requirement, NaCl, which is often used as a stimulator [41], was added to 50 mL of the binary solution (50 mg/L) at pH = 7 in the concentration range of 0.00–0.3 M. The results obtained (Fig. 11) imply that the removal percentage decreases with increase in the salt concentration. This manner, which is consistent with the ones obtained in the analysis of pH effect, can be described based on the competition between the Na^+ ions and the cationic dyes for the same binding sites on the adsorbent surface [5]. Increasing the ionic strength of the solution led to condense the electrical double layer surrounding the adsorbent surface, and therefore, prevent the approach of dye molecules through electrostatic forces [5,42]. To resolve this problem, one can utilize a more quantity of CMPCP.

Table 7
Values for multi-component isotherm constants in a binary system

Isotherms	Parameters	Dye	
		SO	MV
Sheindorf–Rebuhn–Sheintuch	a_{ij}	0.951	1.238
	R^2	0.5355	0.9427
	RMSE	23.04	8.23
Extended-Langmuir	q_{max}	112.30	116.70
	$k_{l,1}$	0.5733	0.4597
	$k_{l,2}$	5.54×10^{-13}	1.46×10^{-13}
	R^2	0.9085	0.9946
	RMSE	11.43	2.83

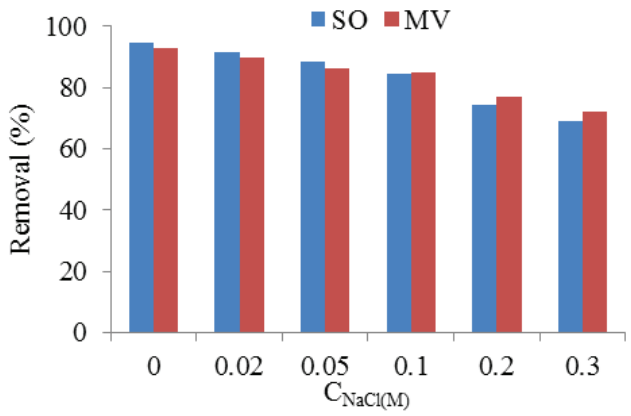

Fig. 11. Effect of ionic strength on removal percentage of SO and MV.

3.6. Possible mechanism

Based upon the structure of the dyes, the functional groups (confirmed by the FT-IR spectra), and the kinetic studies, the possible mechanism can be expressed as follows:

(i) Movement of dye molecules from bulk of the solution to the boundary layer of the adsorbent and accumulation on the surface of CMPCP.
(ii) Adsorption of the molecules on the active sites of CMPCP via electrostatic forces and Van der Waals forces or formation of hydrogen bonds between the nitrogen atoms present in the structure of the dyes and the carboxyl or hydroxyl substituents present on the surface of CMPCP.
(iii) Intra-particle diffusion of dye species into the pores of CMPCP.

Consequently, based on the above-mentioned steps, both the physical and chemical forces are involved in the adsorption of the cited cationic dyes.

3.7. Regeneration of prepared adsorbent

As mentioned earlier, there is a competition between H^+ ions and the cationic dyes for binding to the carboxyl groups present on the adsorbent. Consequently, for regeneration of the exhausted bio-sorbent, HCl (0.1 M) was used as the eluent. Due to the high solubility of the dye molecules in organic solvents [43] and the competition between Na^+ ions and the cationic dyes for the same binding sites on the adsorbent surface, the NaOH–ethanol solution was also selected as the regenerating solvent. The results obtained showed that the re-adsorption efficiency reduced to 65% after the first regeneration cycle with HCl. Du et al. [44] have attributed this effect to the damage of ester bonding in acidic solution, while the adsorption efficiency was 80% even after three cycles with NaOH–ethanol. Thus the adsorbent shows a suitable efficiency with NaOH–ethanol, as the eluent.

3.8. Modeling

3.8.1. Modeling simultanous removal of SO and MV in a binary solution by artificial neural network model

Nowadays, the ANN has attracted much attention for modeling adsorption processes to attain experimental information for designing new large-scale processes [45]. The ANN has the ability to simulate the relationships between input and output data using examples provided to it [5]. A full and detailed discussion of the ANN model has been given in our previous works [5,16,46].

In this work, a fully-connected three-layer feed-forward ANN with error back-propagation learning algorithm that undergoes supervised training was employed to predict the removal percentage of SO and MV in their binary mixture as a function of the pH, adsorbent dosage, initial concentration, and contact time. The architecture of this network is shown in Fig. 12. As one can see in this figure, the first layer with four neurons, which relates to the pH (3, 5, and 7), adsorbent dosage (0.015, 0.025, and 0.035 g), initial concentration (20, 50, 90, and 130 mg/L), and contact time (1–25 min), is recognized

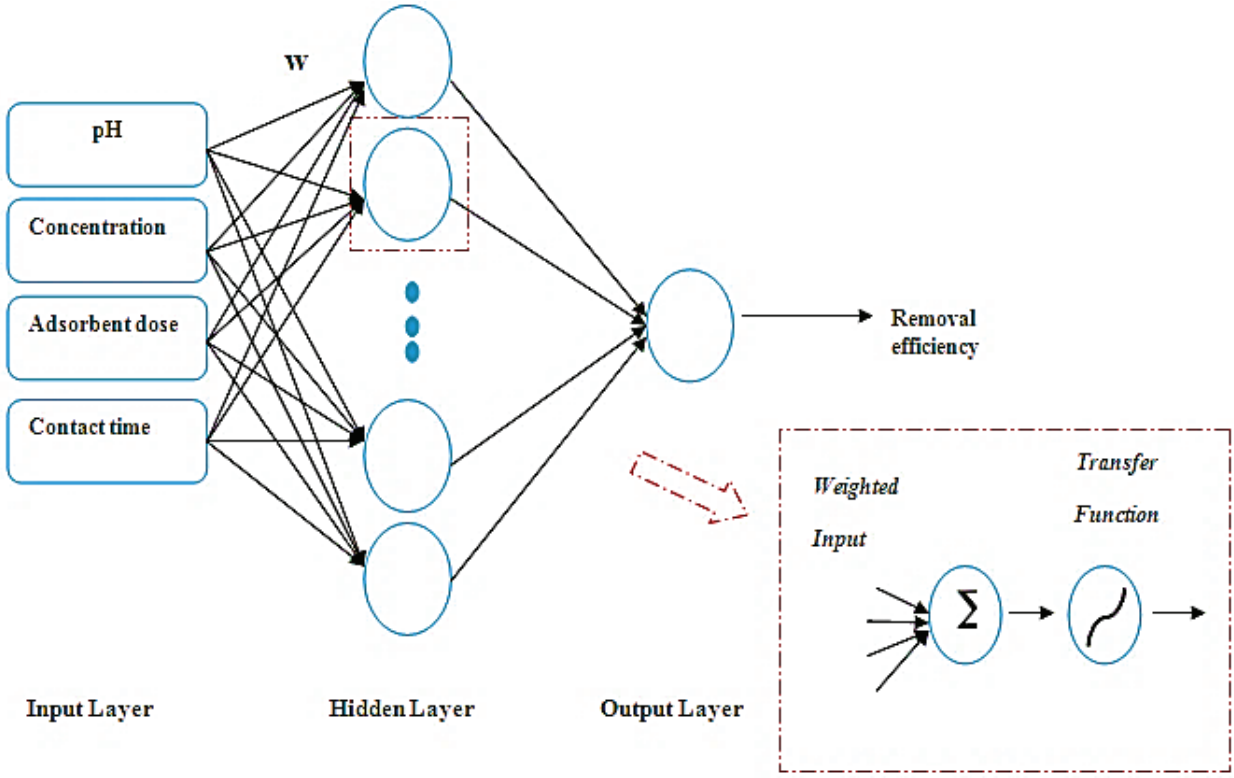

Fig. 12. Topology of ANN model.

as the input layer. The second layer is named as the hidden layer (whose number of neurons must be optimized). The last layer with one neuron, which matches to the removal percentage, is known as the output layer. Connection of the neurons of each layer to the neurons of the subsequent layer is made by an adjustable parameter called weight. In these networks, the output y_i is calculated based on Eq. (12):

$$y_i = f_0\left(\sum_j f_h\left(\sum_i x_i w_{ij} + b_j\right) w_{j1} + b_1\right) \quad (12)$$

where i denotes the ith neuron in the input layer; j is the jth neuron in the hidden layer; f_0 and f_h are the activation functions for the output and hidden layers, respectively; w_{ij} is the weight connecting the ith neuron to the jth neuron; w_{j1} is the weight between the jth neuron in the hidden layer to the neuron in the output layer; and b_j and b_1 are the bias for neuron j and output neuron, respectively. During the training process with different training algorithms, the weights and biases were changed to minimize the error between the predicted and real y_i.

3.8.1.1. Optimization of ANN parameters In order to select the most suitable ANN model, the factors affecting the ANN performance such as the number of neurons available in the hidden layer, type of training function, and transfer function must be optimized. For this requirement, the data set (comprising of 324 data points) was randomly separated into the training set (75%) and test set (25%), respectively [47]. The training set was used to train and optimize the weights and biases by the leave-one-out cross-validation technique [5,46]. According to this procedure, one sample was removed from the training set, and the network was trained using the remaining 242 samples, and then used for prediction of the removed sample. The process was reiterated for the 243 samples available in the training set. Then the mean sum square error (MSE) between the experimental removal percentage (y_i) and the predicted one $\hat{Y}$ was calculated based on Eq. (13) for all the existing samples (N) in the training set, and the optimal values for the ANN factors were determined based on the minimization of this parameter [5].

$$\text{MSE} = \frac{\sum_{i=1}^{N}(y_i - \hat{y}_i)^2}{N} \quad (13)$$

Unfortunately, there were no theoretical or empirical rules that could enable us to determine the number of hidden layers. However, for most ANN applications, one hidden layer can interpret any input–output structure [5,46]. Thus a three-layer ANN including the input, output, and one hidden layer was selected in this work. To optimize the values for the remaining factors, different ANN configurations with different node values in the hidden layer (from 2 to 10), various training functions such as Levenberg–Marquardt (LM), Bayesian regularized (BR), scaled conjugate gradient (SCG), and non-linear transfer functions (as the hyperbolic tangent or logarithmic sigmoid) were constructed, and MSE minimization of the training set was selected as a criterion in the optimization of parameters. According to the results obtained (Tables 8 and 9), the ANN configuration having the LM training function and non-linear hyperbolic tangent function had the lowest MSE for both dyes.

3.8.2. Modeling simultaneous removal of SO and MV in a binary solution by RF model

The RF model is an ensemble machine learning technique proposed by Breiman. This method was developed based on a combination of a lot of unpruned regression trees [48]. Each tree is grown on a separate training dataset that is a bootstrap replicate of the original data [49]. In each bootstrap sample, the data is randomly split into the in-bag data (for training the RF model) and out-of-bag (OOB) data (for evaluation of the prediction error of the model).

The adjustable parameters of this algorithm are ntree, mtry, and node size. The ntree parameter refers to the number of regression trees, while mtry and node size are the number of input variables (predictors) and the minimum size of terminal nodes, respectively [14,15].

The stages of accomplishment of an RF regression model can be described as follows:

(i) Among the training data, around two-third of samples were chosen as the bootstrap sample (in-bag samples) with random replacement, and 1/3 of samples were left-out as the OOB data.
(ii) Decision trees were created using the in-bag samples, and at each node of them, a small random subset of variables (mtry) was selected instead of using all the input variables. This subset has the most suitable split of the feature space.
(iii) The node size variable was initialized, and a regression model was created based on the ntree, mtry, and node size variables.
(iv) Prediction of the desired quantity was carried out using each tree for all the existing examples in the OOB subset.
(v) The results obtained, which were predicted by each tree for each example in the OOB subset, were averaged and used as the final predicted output.
(vi) MSE was then calculated for the OOB subset.
(vii) The above steps were repeated, and the optimal values for ntree, mtry, and node size were determined by minimizing MSE for the OOB subset.

Consequently, based on the steps mentioned, the training subset was divided into the in-bag subset and OOB subset. The input variables (predictors) to RF were pH, adsorbent dosage, initial concentration, and contact time. The output variable was the removal percentage (R). Then at different values of the node size (from 2 to 9), ntree and mtry simultaneously changed ranging from 25 to 500 (with a step size of 25) and from 1 to 4 (with a step size of 1.0), respectively, and the criterion in the optimization of the mentioned factors was minimization of the MSE of OOB samples. MSE of the OOB subset at a fixed value of node size = 2 and different values of ntree and mtry are shown in Fig. 13. According to these figures, for SO at ntree = 150 and mtry = 2, MSE of the OOB data was lessened (Fig. 13(A)), whereas for MV at ntree = 275 and mtry = 2, MSE of the OOB data was minimized (Fig. 13(B)).

Table 8
Minimum MSEs of ANNs at different training algorithms and transfer functions for prediction removal percentage of SO

No.	Input layer nodes	Hidden layer nodes	Training algorithm	Transfer function	MSE
1	4	4	BR	tansig	7.68
2	4	7	BR	logsig	10.96
3	4	8	LM	tansig	4.60
4	4	8	LM	logsig	10.49
5	4	6	SCG	tansig	31.49
6	4	6	SCG	logsig	55.43

Table 9
Minimum MSEs of ANNs at different training algorithms and transfer functions for prediction removal percentage of MV

No.	Input layer nodes	Hidden layer nodes	Training algorithm	Transfer function	MSE
1	4	4	BR	tansig	5.72
2	4	9	BR	logsig	7.79
3	4	8	LM	tansig	4.2
4	4	8	LM	logsig	6.74
5	4	5	SCG	tansig	31.94
6	4	6	SCG	logsig	35.52

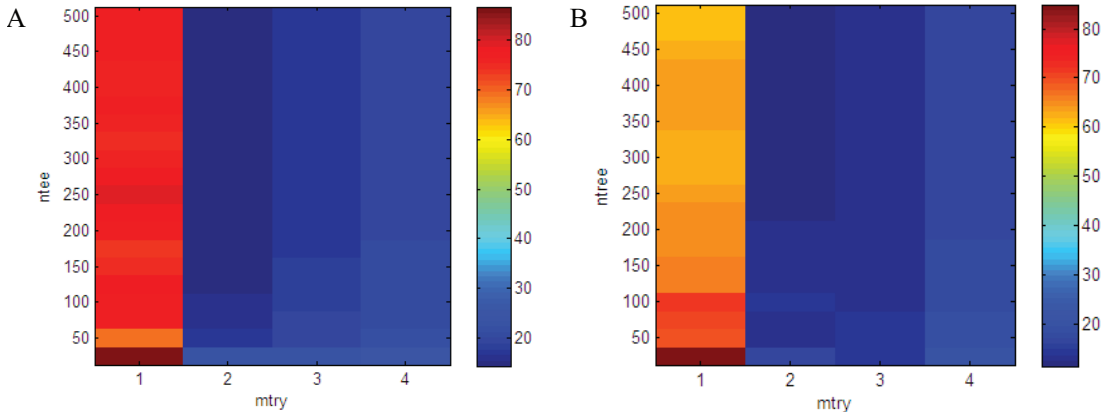

Fig. 13. MSEs of OOB data at node size = 2 and different values of ntree and mtry for (A) SO and (B) MV.

3.8.3. Validation of models created by RF and ANN methods

The predictive ability of a model is its capability to give an acceptable output for a sample that is not presented in the learning samples [5]. In this regard, the optimized RF and ANN models were used to predict the removal percentage of 81 samples in the test set. The accuracy of prediction of the constructed models was examined by different statistical parameters such as MSE, mean relative error (MRE), and R^2, which are defined by Eqs. (13)–(15), respectively.

$$\mathrm{MRE} = \frac{\sum_{i=1}^{N}\left|\frac{(y_i - \hat{y}_i)}{y_i}\right|}{N} \times 100 \tag{14}$$

$$R^2 = 1 - \frac{\sum\left(y_i - \hat{y}\right)^2}{(y_i - \overline{y})^2} \tag{15}$$

Table 10
Statistical parameters for evaluation of accuracy of constructed models in forecasting removal percentage of SO

Parameter	ANN		RF	
	Training	Test set	Training	Test set
MSE	4.61	5.34	4.78	24.68
MRE	4.57	4.88	5.20	11.41
R^2	0.9970	0.9910	0.9957	0.9646

Table 11
Statistical parameters for evaluation of accuracy of constructed models in forecasting removal percentage of MV

Parameter	ANN		RF	
	Training	Test set	Training	Test set
MSE	4.20	5.19	3.81	18.09
MRE	3.90	3.94	4.14	9.43
R^2	0.9933	0.9907	0.9956	0.9748

where y_i, $\hat{y}_i$, and N have been previously defined. The values for these parameters are tabulated in Tables 10 and 11, respectively. Based on these values and Figs. 14 and 15, a comparison between the ANN and RF models demonstrates that the ANN model has a superior ability for prediction of the removal percentage of the cited dyes.

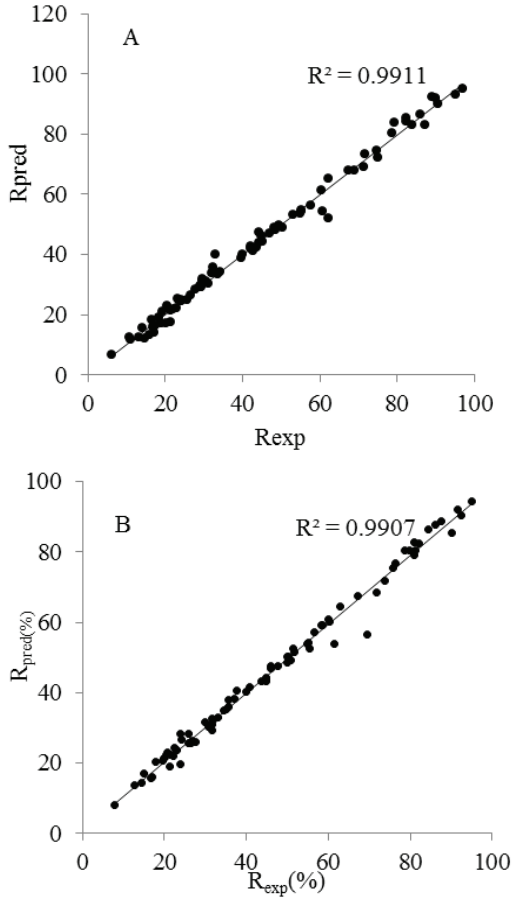

Fig. 14. Plots of predicted against experimental removal percentage values by ANN for (A) SO and (B) MV.

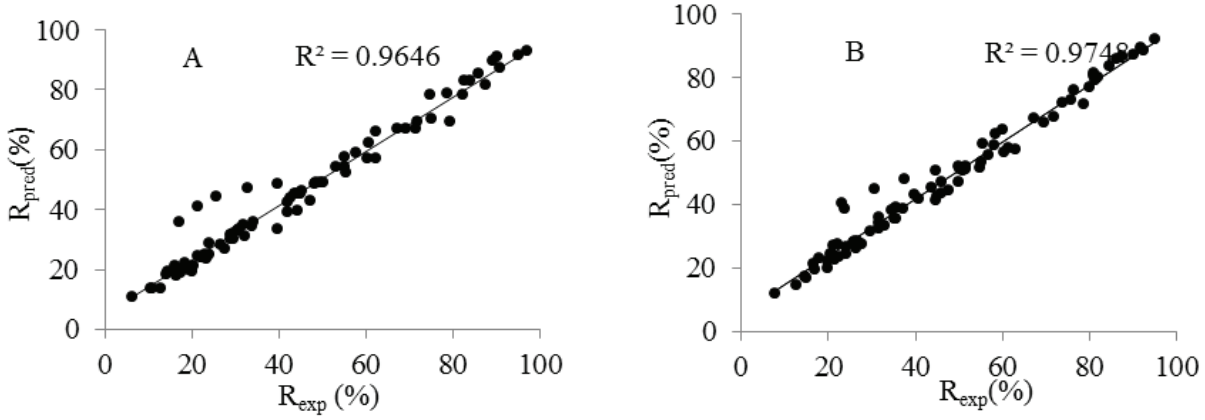

Fig. 15. Plots of predicted against experimental removal percentage values by RF for (A) SO and (B) MV.

4. Conclusion

CMPCP, as a low-cost and available adsorbent, was succesfully used for the removal of the SO and MV dyes from single and binary solutions. The high surface area and the functional groups present on CMPCP are resposible for the rapid adsorption of the dyes. Analysis of the equilibrium data using different isotherms demostrated that the adsorption nature of the cited dyes onto CMPCP was more compatible with the Langmuir model, and the kinetic of adsorption was satisfactorily predicted by a pseudo-second order model. Also with respect to the other proposed adsorbent, CMPCP displayed a similar or an even better performance. Exhausted CMPCP was recoverd using NaOH–ethanol (1%), and the investigation showed that after four adsorption–regeneration cycles, the regeneration efficiency was at a high level. Moreover, modeling the removal percentage as a function of the experimental parameters using the ANN and RF methods indicated that the ANN method had a higher ability in modeling. This results obtained implied that there was a non-linear relationship between the experimental parameters and the removal efficiency.

Acknowledgment

The authors are thankful to the Shahrood University of Technology Research Council for the support of this work.

References

[1] M. Arshadi, A.R. Faraji, M.J. Amiri, M. Mehravar, A. Gil, Removal of methyl orange on modified ostrich bone waste–a novel organic-inorganic biocomposite, J. Colloid Interface Sci., 446 (2015) 11–23.
[2] M. Ghaedi, S. Hajati, B. Barazesh, F. Karimi, G. Ghezelbash, *Saccharomyces cerevisiae* for the biosorption of basic dyes from binary component systems and the high order derivative spectrophotometric method for simultaneous analysis of Brilliant green and Methylene blue, J. Ind. Eng. Chem. Res., 19 (2013) 227–233.
[3] U.A. Guler, M.E. Eliza, T.F. Dügenci, Mono and simultaneous removal of crystal violet and safranin dyes from aqueous solutions by HDTMA-modified Spirulina sp., J. Process Saf. Environ. Prot., 99 (2016) 194–206.
[4] G.Z. Kyzas, N.K. Lazaridis, M. Kostoglou, On the simultaneous adsorption of a reactive dye and hexavalent chromium from aqueous solutions onto grafted chitosan, J. Colloid Interface Sci., 407 (2013) 432–441.
[5] M. Ashrafi, M.A. Chamjangali, G. Bagherian, N. Goudarzi, Application of linear and non-linear methods for modeling removal efficiency of textile dyes from aqueous solutions using magnetic Fe_3O_4 impregnated onto walnut shell, Spectrochim. Acta Part A, 171 (2017) 268–279.
[6] S. Chakraborty, S. Chowdhury, P.D. Saha, Adsorption of crystal violet from aqueous solution onto NaOH-modified rice husk, Carbohydr. Polym., 86 (2011) 1533–1541.
[7] P. Sharma, H. Kaur, M. Sharma, V. Sahore, A review on applicability of naturally available adsorbents for the removal of hazardous dyes from aqueous waste, Environ. Monit. Assess., 183 (2011) 151–195.
[8] R. Slimani, I. El Ouahabi, F. Abidi, M. El Haddad, A. Regti, M.R. Laamari, S. Lazar, Calcined eggshells as a new biosorbent to remove basic dye from aqueous solutions: thermodynamics, kinetics, isotherms and error analysis, J. Taiwan Inst. Chem. Eng., 45 (2014) 1578–1587.
[9] G.Z. Kyzas, P.I. Siafaka, E.G. Pavlidou, K.J. Chrissafis, D.N. Bikiaris, Synthesis and adsorption application of succinyl-grafted chitosan for the simultaneous removal of zinc and cationic dye from binary hazardous mixtures, Chem. Eng. J., 259 (2015) 438–448.
[10] B. Chen, Y. Liu, S. Chen, X. Zhao, X. Meng, X. Pan, Magnetically recoverable cross-linked polyethylenimine as a novel adsorbent for removal of anionic dyes with different structures from aqueous solution, J. Taiwan Inst. Chem. Eng., 67 (2016) 191–201.
[11] B.C.S. Ferreira, F.S. Teodoro, A.B. Mageste, L.F. Gil, R.P. de Freitas, L.V.A. Gurgel, Application of a new carboxylate-functionalized sugarcane bagasse for adsorptive removal of crystal violet from aqueous solution: kinetic, equilibrium and thermodynamic studies, J. Ind. Eng. Chem., 65 (2015) 521–534.
[12] G.J. Ehlert, Y. Lin, H.A. Sodano, Carboxyl functionalization of carbon fibers through a grafting reaction that preserves fiber tensile strength, Carbon, 49 (2012) 4246–4255.
[13] A. Çelekli, H. Bozkurt, F. Geyik, Use of artificial neural networks and genetic algorithms for prediction of sorption of an azo-metal complex dye onto lentil straw, Bioresour. Technol., 129 (2013) 396–401.
[14] M. Ashrafi, M.A. Chamjangali, G. Bagherian, N. Goudarzi, Evaluation of nanosilica, extracted from stem sweep, as a new adsorbent for simultaneous removal of crystal violet and methylene blue from aqueous solutions, Desal. Wat. Treat., 88 (2017) 207–220.
[15] F. Heydari, M. Ghaedi, A. Ansari, A.M. Ghaedi, Random forest model for removal of methylene blue and lead (II) ion using activated carbon obtained from Tamarisk, Desal. Wat. Treat., 57 (2016) 19273–19291.
[16] A.M. Ghaedi, A. Vafaei, Applications of artificial neural networks for adsorption removal of dyes from aqueous solution: a review, Adv. Colloid Interface Sci., 245 (2016) 20–39.
[17] N.H. Singh, K. Kezo, A. Debnath, B. Saha, Enhanced adsorption performance of a novel Fe-Mn-Zr metal oxide nanocomposite adsorbent for anionic dyes from binary dye mix: response surface optimization and neural network modeling, Appl. Organomet. Chem., (2017). DOI: 10.1002/aoc.4165.
[18] J. Zolgharnein, M. Bagtash, T. Shariatmanesh, Simultaneous removal of binary mixture of Brilliant Green and Crystal Violet using derivative spectrophotometric determination, multivariate optimization and adsorption characterization of dyes on surfactant modified nano-γ-alumina, Spectrochim. Acta Part A, 137 (2015) 1016–1028.
[19] J.F. Gao, J.H. Wang, C. Yang, S.Y. Wang, Y.Z. Peng, Binary biosorption of Acid Red 14 and Reactive Red 15 onto acid treated okara: simultaneous spectrophotometric determination of two dyes using partial least squares regression, Chem. Eng. J., 171 (2011) 967–975.
[20] J.B. Nevado, J.R. Flores, M.V. Llerena, N.R. Fariñas, Simultaneous spectrophotometric determination of tartrazine, patent blue V, and indigo carmine in commercial products by partial least squares and principal component regression methods, Talanta, 48 (1999) 895–903.
[21] S. Wold, M. Sjostrom, L. Eriksson, PLS-regression: a basic tool of chemometrics, Chemom. Intell. Lab. Syst., 58 (2001) 109–130.
[22] A. Niazi, A. Yazdanipour, Spectrophotometric simultaneous determination of nitrophenol isomers by orthogonal signal correction and partial least squares, J. Hazard. Mater., 146 (2007) 421–427.
[23] M. Arab Chamjangali, G.A. Bagherian, G. Azizi, Simultaneous determination of cobalt, nickel and palladium in micellar media using partial least square regression and direct orthogonal signal correction, Spectrochim. Acta Part A, 62 (2005) 189–196.
[24] M. Peydayesh, A. Rahbar-Kelishami, Adsorption of methylene blue onto *Platanus orientalis* leaf powder: kinetic, equilibrium and thermodynamic studies, J. Ind. Eng. Chem., 21 (2015) 1014–1019.
[25] A. Saeed, M. Sharif, M. Iqbal, Application potential of grapefruit peel as dye sorbent: kinetics, equilibrium and mechanism of crystal violet adsorption, J. Hazard. Mater., 179 (2010) 564–572.
[26] J.S. Cao, J.X. Lin, F. Fang, M.T. Zhang, Z.R. Hu, A new absorbent by modifying walnut shell for the removal of anionic dye: kinetic and thermodynamic studies, Bioresour. Technol., 163 (2014) 199–205.

[27] A. Chadlia, K. Mohamed, L. Najah, Preparation and characterization of new succinic anhydride grafted Posidonia for the removal of organic and inorganic pollutants, J. Hazard. Mater., 172 (2009) 1579–1590.
[28] C.F. Liu, R.C. Sun, M.H. Qin, A.P. Zhang, J.L. Ren, J. Ye, Z.N. Cao, Succinoylation of sugarcane bagasse under ultrasound irradiation, Bioresour. Technol., 99 (2008) 1465–1473.
[29] S. Hokkanen, E. Repo, M. Sillanpää, Removal of heavy metals from aqueous solutions by succinic anhydride modified mercerized nanocellulose, Chem. Eng. J., 223 (2013) 40–47.
[30] F.Z. Arrakhiz, M. El Achaby, K. Benmoussa, R. Bouhfid, M. Essassi, A. Qaiss, Evaluation of mechanical and thermal properties of Pine cone fibers reinforced compatibilized polypropylene, Mater. Design, 40 (2012) 528–535.
[31] A.E. Ofomaja, E.B. Naidoo, Biosorption of copper from aqueous solution by chemically activated pine cone: a kinetic study, Chem. Eng. J., 175 (2011) 260–270.
[32] J.Z. Guo, B. Li, L. Liu, K. Lv, Removal of methylene blue from aqueous solutions by chemically modified bamboo, Chemosphere, 111 (2014) 225–231.
[33] S. Banerjee, G.C. Sharma, R.K. Gautam, M.C. Chattopadhyaya, S.N. Upadhyay, Y.C. Sharma, Removal of Malachite Green, a hazardous dye from aqueous solutions using *Avena sativa* (oat) hull as a potential adsorbent, J. Mol. Liq., 213 (2016) 162–172.
[34] M.R. Malekbala, M.A. Khan, S. Hosseini, L.C. Abdullah, T.S. Choong, Adsorption/desorption of cationic dye on surfactant modified mesoporous carbon coated monolith: equilibrium, kinetic and thermodynamic studies, J. Ind. Eng. Chem., 21 (2015) 369–377.
[35] T. Madrakian, A. Afkhami, M. Ahmadi, Adsorption and kinetic studies of seven different organic dyes onto magnetite nanoparticles loaded tea waste and removal of them from wastewater samples, Spectrochim. Acta Part A, 99 (2012) 102–109.
[36] B.H. Hameed, Evaluation of papaya seeds as a novel non-conventional low-cost adsorbent for removal of methylene blue, J. Hazard. Mater., 162 (2009) 939–944.
[37] N.M. Mahmoodi, R. Salehi, M. Arami, Binary system dye removal from colored textile wastewater using activated carbon: kinetic and isotherm studies, Desalination, 272 (2011) 187–195.
[38] M. Ghaedi, S. Hajjati, Z. Mahmudi, I. Tyagi, S. Agarwal, A. Maity, V.K. Gupta, Modeling of competitive ultrasonic assisted removal of the dyes–Methylene blue and Safranin-O using Fe_3O_4 nanoparticles, Chem. Eng. J., 268 (2015) 28–37.
[39] K.V. Kumar, A. Kumaran, Removal of methylene blue by mango seed kernel powder, Biochem. J., 27 (2005) 83–93.
[40] M. Turabik, Adsorption of basic dyes from single and binary component systems onto bentonite: simultaneous analysis of Basic Red 46 and Basic Yellow 28 by first order derivative spectrophotometric analysis method, J. Hazard. Mater., 158 (2008) 52–64.
[41] M. Ghaedi, H. Hossainian, M. Montazerozohori, A. Shokrollahi, F. Shojaipour, M. Soylak, M.K. Purkait, A novel acorn based adsorbent for the removal of brilliant green, Desalination, 281 (2011) 226–233.
[42] Z. Aksu, E. Balibek, Effect of salinity on metal-complex dye biosorption by *Rhizopus arrhizus*, J. Environ. Manage., 91 (2010) 1546–1555.
[43] F. Ge, H. Ye, M.M. Li, B.X. Zhao, Efficient removal of cationic dyes from aqueous solution by polymer-modified magnetic nanoparticles, Chem. Eng. J., 198 (2012) 11–17.
[44] Z. Du, T. Zheng, P. Wang, L. Hao, Y. Wang, Fast microwave-assisted preparation of a low-cost and recyclable carboxyl modified lignocellulose-biomass jute fiber for enhanced heavy metal removal from water, Bioresour. Technol., 201 (2016) 41–49.
[45] G.K. Parshetti, S. Chowdhury, R. Balasubramanian, Hydrothermal conversion of urban food waste to chars for removal of textile dyes from contaminated waters, Bioresour. Technol., 161 (2014) 310–319.
[46] M.A. Chamjangali, M. Ashrafi, QSAR study of necroptosis inhibitory activities (EC_{50}) of [1, 2, 3] thiadiazole and thiophene derivatives using Bayesian regularized artificial neural network and calculated descriptors, Med. Chem. Res., 22 (2013) 392–400.
[47] E.A. Dil, M. Ghaedi, A. Ghaedi, A. Asfaram, M. Jamshidi, M.K. Purkait, Application of artificial neural network and response surface methodology for the removal of crystal violet by zinc oxide nanorods loaded on activate carbon: kinetics and equilibrium study, J. Taiwan Inst. Chem. Eng., 59 (2016) 210–220.
[48] N. Dehghanian, M. Ghaedi, A. Ansari, A. Ghaedi, A. Vafaei, M. Asif, V.K. Gupta, A random forest approach for predicting the removal of Congo red from aqueous solutions by adsorption onto tin sulfide nanoparticles loaded on activated carbon, Desal. Wat. Treat., 57 (2016) 9272–9285.
[49] N. Goudarzi, D. Shahsavani, Application of a random forests (RF) method as a new approach for variable selection and modeling in a QSRR study to predict the relative retention time of some polybrominated diphenylethers (PBDEs), Anal. Methods, 4 (2012) 3733–3738.